Inorg. Chem. **2004**, *43*, 2834–2844

Exchange Coupling of Paramagnetic Ions in a Polyoxometalate Matrix: Density Functional Study of Diiron(III) Substituted γ-Silicotungstates

Ekaterina M. Zueva,[†,§] Henry Chermette,[†,‡] and Serguei A. Borshch*[,†]

Laboratoire de Chimie, UMR 5182 CNRS—Ecole Normale Supérieure de Lyon, 46 allée d'Italie, 69364 Lyon Cedex 07, France, Université Claude Bernard Lyon-1, bat. 210, 43 boulevard 11 novembre 1918, 69622 Villeurbanne Cedex, France, and Department of Inorganic Chemistry, Kazan State Technological University, 68 K. Marx Street, 420015 Kazan, Russia

Received October 7, 2003

The quantum chemical (density functional) analysis of the antiferromagnetic interactions between the two iron centers incorporated into the γ-silicotungstate is performed. The influence of the polyoxometalate framework on the exchange coupling within the diiron core unit is studied. The dependence of the strength of antiferromagnetic exchange on the protonation of the core bridges is considered. It is shown that the magnetic coupling is very sensitive to the distortions in core geometry. Variations in the core structure induced by the environment (such as the polyoxometalate framework) change the significance of superexchange pathways and give rise to new superexchange mechanisms. This effect is especially pronounced in the case of the hydroxo-bridged diiron core.

I. Introduction

Polyoxometalates (POMs) constitute a large group of polynuclear metal−oxygen anionic clusters with unique physical and chemical properties. Due to their high acidity and oxidizing function, POMs find multiple applications in catalysis, both heterogeneous and homogeneous, materials science, and medicine.[1−3] Among many other heteropolyanions, the most stable Keggin structures $[XM_{12}O_{40}]^{n-}$ have been studied more intensively. It has been shown that the properties of polyanions can be significantly modified by substitution of a main metal atom (M) by another metal atom (M′). Recently, Mizuno et al.[4,5] have studied the activity of non-, mono-, di-, and triiron substituted Keggin type silicotungstates (α-$[SiW_{12}O_{40}]^{4-}$, α-$[SiW_{11}Fe(OH_2)O_{39}]^{5-}$, γ-$[SiW_{10}\{Fe(OH_2)\}_2O_{38}]^{6-}$, and α-$[SiW_9\{Fe(OH_2)\}_3O_{37}]^{7-}$) as catalysts for the oxygenation of alkanes (including methane) in homogeneous reaction media. The authors have reported that incorporation of iron centers into the POM framework remarkably influences the catalytic activity. Interestingly, the diiron substituted derivative γ-$[SiW_{10}\{Fe(OH_2)\}_2O_{38}]^{6-}$ (**I**) appears to be the most active. Different spectroscopic methods have been used to characterize this polyanion. The results of these studies suggest that **I** has a γ-Keggin structure with C_{2v} symmetry and that the two iron atoms occupy adjacent, edge-sharing octahedra, forming a di-μ-oxo-bridged diiron(III) unit (Figure 1). However, no more structural details of **I** have been ascertained, as it was not crystallographically characterized. Magnetic susceptibility measurement reveals that the two high-spin iron centers are involved in a weak antiferromagnetic coupling, with the value of the exchange coupling constant, J, in the range -5 to -1 cm^{-1}. As the J value and Mössbauer spectroscopy parameters for **I** are more close to those for high-spin diferric complexes with hydroxo-bridged core architecture, it has been assumed that **I** may have a μ-hydroxo diiron structure. Moreover, the Mössbauer and magnetic data for **I** appear to be similar to those for the resting (oxidized) form of the hydroxylase component of the methane monooxygenase ($MMOH_{ox}$),

* Corresponding author. E-mail: borchtch@catalyse.cnrs.fr.
† CNRS—Ecole Normale Supérieure de Lyon.
‡ Université Claude Bernard Lyon-1.
§ Kazan State Technological University.

(1) *Polyoxometalates: From Platonic Solids to Anti-Retroviral Activity*; Pope, M. T., Müller, A., Eds.; Kluwer Academic Publishers: Dordrecht, The Netherlands, 1994.
(2) Special Issue on Polyoxometalates; Hill, C. L., Ed. *Chem. Rev.* **1998**, *98*, N1.
(3) *Polyoxometalate Chemistry: From Topology via Self-Assembly to Applications*; Pope, M. T., Müller, A., Eds.; Kluwer Academic Publishers: Dordrecht, The Netherlands, 2001.
(4) Mizuno, N.; Nozaki, C.; Kiyoto, I.; Misono, M. *J. Am. Chem. Soc.* **1998**, *120*, 9267.
(5) Nozaki, C.; Kiyoto, I.; Minai, Y.; Misono, M.; Mizuno, N. *Inorg. Chem.* **1999**, *38*, 5724.

10.1021/ic035161t CCC: $27.50
Published on Web 04/01/2004

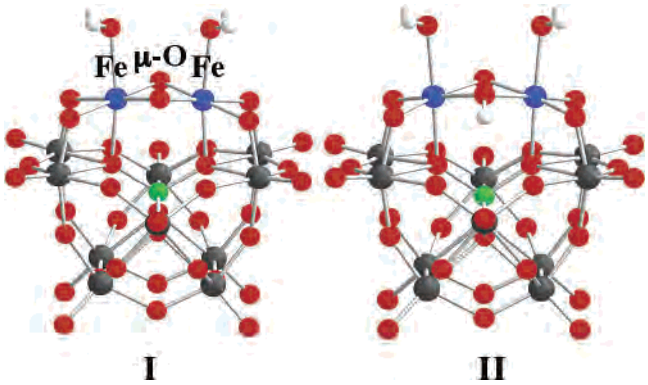

Figure 1. Ball-and-stick representation of the di-μ-oxo- and di-μ-hydroxo-bridged diiron(III) substituted γ-silicotungstates.

whose active site has already been shown to contain a diiron core with hydroxo- and aqua-bridging ligands.[6−8] On this basis, the authors have proposed that the remarkable catalytic performance of diiron substituted γ-silicotungstates may be related to the catalysis by methane monooxygenase.

The role of the $Fe_2(\mu\text{-}O)_2$ core in the oxygen reactivity of non-heme iron protein and enzyme systems is not completely elucidated. It is supposed that these systems utilize such core structures to access the iron(IV) oxidation state.[9] For instance, the high-valent intermediate Q in the catalytic cycle of MMOH is assumed to contain this unit.[10,11] A number of theoretical studies have been undertaken to construct a model of Q and to propose a mechanism of a reaction occurring at its active site.[12,13] Recently, an example of a high-valent diiron core, namely, the $[Fe^{III}Fe^{IV}(\mu\text{-}O)_2]^{3+}$ complex, has been crystallized,[14] and a combination of spectroscopic methods and density functional calculations has been used to determine the electronic and geometric features of this core and to discuss its possible relevance to the high-valent binuclear non-heme enzyme intermediates.[15] It cannot be excluded that the $Fe_2(\mu\text{-}O)_2$ core and its protonated analogues, $Fe_2(\mu\text{-}OH_n)(\mu\text{-}OH_m)$, may be found in the active sites of non-heme iron enzymes also in the diiron(III) oxidation state, as it occurs in $MMOH_{ox}$. A few examples of such cores have been synthesized and characterized.[16,17] The diiron(III) complexes with $Fe_2(\mu\text{-}O)_2$ and $Fe_2(\mu\text{-}O)(\mu\text{-}OH)$ units were examined, and their structural, electronic, and magnetic properties were found to be quite distinct from those of the more common diiron(III) derivatives with a single μ-oxo bridge. The authors have stressed that these peculiarities can serve as useful tools to ascertain the presence of such units in metalloenzyme active sites. A more profound understanding of the nature of electronic interactions within these diiron(III) core structures can be attained by using quantum chemical techniques. To our knowledge, only two quantum-mechanics-based studies of the systems containing such diiron(III) core units have been reported in the literature. In the work of Caneschi et al.[18] dealing with the di-μ-hydroxo(alkoxo)-bridged diiron(III) complexes, density functional calculations were carried out to deduce the dependence of magnetic coupling on the geometry of dimers. Noodleman et al.[19] examined several cluster models of the $MMOH_{ox}$ active site to assess the identity of the oxygen-based bridging ligands in the diiron(III) core unit within $MMOH_{ox}$. However, none of these two studies presents a detailed analysis of the electronic structures of the systems. It should be mentioned that thorough molecular orbital (MO) studies have been already carried out for the μ-oxo-di-μ-carboxylato-bridged diiron(III) complexes considered as models of the hemerythrin active site[20,21] and systems containing a dimanganese unit in different oxidation states having relevance to the oxygen-evolving complex of photosystem II.[22,23]

As it can be seen, magnetochemical methods play an important role in the characterization and the comparison of biomimetic complexes and natural systems. They are also widely used in the studies of transition metal substituted POM systems. The importance of these methods is directly linked with applications of POMs in the field of the molecule-based materials.[24] The ability of the POM framework to accommodate one or several magnetic centers at specific positions enables the design of novel molecular materials combining useful electric and magnetic properties. A number of addenda nonsubstituted α-Keggin anions $[X^{n+}W_{12}O_{40}]^{(8-n)-}$ with paramagnetic heteroatoms ($X = Cu^{II}$, Co^{II}, Fe^{III}, etc.), addenda monosubstituted α-Keggin anions $[X^{n+}Z^{m+}(OH_2)M_{11}O_{39}]^{(12-n-m)-}$ ($Z = Fe^{III}$, Cr^{III}, Mn^{II}, etc.), and some more complicated polyanions have been already tested in this respect. Theoretical studies of magnetic coupling between paramagnetic ions in the parent POM component would be helpful in the rationalization of the observed properties of the POM system in itself and in the design of new, interesting POM-based molecular magnetic materials.

(6) Rosenzweig, A. C.; Frederick, C. A.; Lippard, S. J.; Nordlund, P. *Nature* **1993**, *366*, 537.
(7) Rosenzweig, A. C.; Nordlund, P.; Takahara, P. M.; Frederick, C. A.; Lippard, S. J. *Chem. Biol.* **1995**, *2*, 409.
(8) Elango, N.; Radhakrishnan, R.; Froland, W. A.; Wallar, B. J.; Earhart, C. A.; Lipscomb, J. D.; Ohlendorf, D. H. *Protein Sci.* **1997**, *6*, 556.
(9) Solomon, E. I.; Brunold, T. C.; Davis, M. I.; Kemsley, J. N.; Lee, S.-K.; Lehnert, N.; Neese, F.; Skulan, A. J.; Yang, Y.-S.; Zhou, J. *Chem. Rev.* **2000**, *100*, 235 and references therein.
(10) Liu, K. E.; Lippard, S. J. *Adv. Inorg. Chem.* **1995**, *42*, 263 and references therein.
(11) Wallar, B. J.; Lipscomb, J. D. *Chem. Rev.* **1996**, *96*, 2625 and references therein.
(12) Baik, M.-H.; Newcomb, M.; Friesner, R. A.; Lippard, S. J. *Chem. Rev.* **2003**, *103*, 2385 and references therein.
(13) Lovell, T.; Han, W.-G.; Liu, T.; Noodleman, L. *J. Am. Chem. Soc.* **2002**, *124*, 5890.
(14) Hsu, H.-F.; Dong, Y. H.; Shu, L. J.; Young, V. G., Jr.; Que, L., Jr. *J. Am. Chem. Soc.* **1999**, *121*, 5230.
(15) Skulan, A. J.; Hanson, M. A.; Hsu, H.-F.; Que, L., Jr.; Solomon, E. I. *J. Am. Chem. Soc.* **2003**, *125*, 7344.
(16) Zang, Y.; Dong, Y.; Que, L., Jr.; Kauffmann, K.; Münck, E. *J. Am. Chem. Soc.* **1995**, *117*, 1169.
(17) Zheng, H.; Zang, Y.; Dong, Y.; Young, V. G., Jr.; Que, L., Jr. *J. Am. Chem. Soc.* **1999**, *121*, 2226.
(18) Caneschi, A.; Biani, F. F.; Kloo, L.; Zanello, P. *Int. J. Quantum Chem.* **1999**, *72*, 61.
(19) Lovell, T.; Li, J.; Noodleman, L. *Inorg. Chem.* **2001**, *40*, 5251.
(20) Brown, C. A.; Remar, G. J.; Musselman, R. L.; Solomon, E. I. *Inorg. Chem.* **1995**, *34*, 688.
(21) Rodriguez, J. H.; McCusker, J. K. *J. Chem. Phys.* **2002**, *116*, 6253.
(22) Zhao, X. G.; Richardson, W. H.; Chen, J.-L.; Li, J.; Noodleman, L.; Tsai, H.-L.; Hendrickson, D. N. *Inorg. Chem.* **1997**, *36*, 1198.
(23) McGrady, J. E.; Stranger, R. *J. Am. Chem. Soc.* **1997**, *119*, 8512.
(24) Coronado, E.; Gómez-García, C. J. *Chem. Rev.* **1998**, *98*, 273 and references therein.

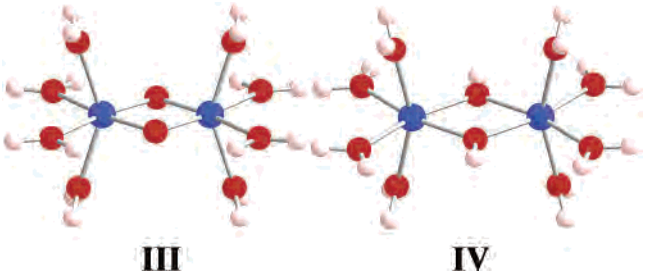

Figure 2. Ball-and-stick representation of the di-μ-oxo- and di-μ-hydroxo-bridged diiron(III) complexes.

Both aspects, the proposed analogy between the diiron core in **I** and the active site of the methane monooxygenase on one side and a special interest in the nature of magnetic coupling in POMs on the other side, suggest the importance of the quantum chemical analysis of the di-μ-oxo- and di-μ-hydroxo-bridged diiron(III) substituted γ-silicotungstates (**I** and **II** vide infra, Figure 1). Numerous ab initio and density functional calculations on POM systems are known in the literature.[25−30] However, the magnetic properties have been considered only for reduced (blue) species. The present paper provides a description of the exchange coupling between two magnetic centers in the POM framework. We present a detailed analysis of the electronic structure and magnetic properties of polyanions **I** and **II** using a density functional computational scheme. In both systems, the magnetic properties are determined by the superexchange interactions between the iron centers. The superexchange pathways giving rise to molecular antiferromagnetism have been identified, and their modification following protonation of the oxo bridges has been studied. To investigate the influence of the POM framework on the formation of superexchange pathways and on the strength of antiferromagnetic exchange, we performed analogous calculations on the free di-μ-oxo- and di-μ-hydroxo-bridged diiron(III) complexes $[Fe_2(\mu\text{-}O)_2(OH_2)_8]^{2+}$ and $[Fe_2(\mu\text{-}OH)_2(OH_2)_8]^{4+}$ (**III** and **IV** vide infra, Figure 2).

II. Theoretical Details

Density functional theory is a monodeterminantal method, and its spin-restricted singlet solution is not supposed to provide an adequate description of the ground state of antiferromagnetically coupled systems, where magnetic α- and β-electrons are not completely delocalized. The broken-symmetry (BS) technique developed by Noodleman et al.[31−34] has proved to be a powerful approach for treating such systems.[35−44] Although the BS state is a mixed spin state with $M_S = 0$, it is generally considered that the monodeterminantal BS solution is a reasonable approximation to the ground state of antiferromagnetically coupled systems.

The exchange coupling constant, J, appearing in the Heisenberg−Dirac−Van Vleck spin Hamiltonian, written for two magnetic centers with spins S_1 and S_2 as

$$H = -2JS_1S_2$$

can be determined from the expression derived by Noodleman et al.[31−34] by means of spin-projection technique:

$$E_{HS}(S_{max}) - E_{BS} = -S_{max}{}^2J$$

In this formula, $E_{HS}(S_{max})$ and E_{BS} are the energies of the HS (high spin) and BS states, respectively. It has been figured out[42−44] that $S_{max} = S_1 + S_2$ only if all unpaired (magnetic) electrons can be treated as being weakly antiferromagnetically coupled. The HS state is a pure spin state described by a single determinant, and its energy can be easily calculated within density functional formalism.

All density functional calculations were carried out with the Amsterdam density functional (ADF) program, version 2000.02,[45] in the spin-unrestricted framework. The Vosko, Wilk, and Nusair exchange-correlation potential[46] was used to construct the local part of the energy functional, and the Becke[47] and Perdew[48] gradient corrections were added to the exchange and correlation energy functionals, respectively. Electrons in the shells up to and including 4f (for W), 2p (for Fe), 2p (for Si), and 1s (for O) were treated within the frozen-core approximation. Scalar quasirelativistic corrections (within the Pauli formalism) were explicitly introduced in the core potentials. The quasirelativistic frozen-core shells were generated by means of the auxiliary program DIRAC.[45]

Taking into account that only the HS state can be accurately represented by a monodeterminantal Kohn−Sham wave function, the geometries of the systems being studied were optimized in their HS states ($S_{max} = 5$). Geometry optimizations were performed using the gradient algorithm of Versluis and Ziegler[49] under the constraints of the C_{2v}

(25) Poblet, J. M.; López, X.; Bo, C. *Chem. Soc. Rev.* **2003**, *32*, 297 and references therein.
(26) Rohmer, M.-M.; Bénard, M.; Blaudeau, J.-P.; Maestre, J. M.; Poblet, J. M. *Coord. Chem. Rev.* **1998**, *178−180*, 1019 and references therein.
(27) Suaud, N.; Gaita-Ariño, A.; Clemente-Juan, J. M.; Sánchez-Marin, J.; Coronado, E. *J. Am. Chem. Soc.* **2002**, *124*, 15134 and references therein.
(28) Maestre, J. M.; Poblet, J. M.; Bo, C.; Casañ-Pastor, N.; Gómez-Romero, P. *Inorg. Chem.* **1998**, *37*, 3444 and references therein.
(29) Bridgeman, A. *Chem. Phys.* **2003**, *287*, 55 and references therein.
(30) Duclusaud, H.; Borshch, S. A. *J. Am. Chem. Soc.* **2001**, *123*, 2825 and references therein.
(31) Noodleman, L.; Norman, J. G., Jr. *J. Chem. Phys.* **1979**, *70*, 4903.
(32) Noodleman, L. *J. Chem. Phys.* **1981**, *74*, 5737.
(33) Noodleman, L.; Case, D. A. *Adv. Inorg. Chem.* **1992**, *38*, 423.
(34) Noodleman, L.; Davidson, E. R. *Chem. Phys.* **1986**, *109*, 131.
(35) Aizman, A.; Case, D. A. *J. Am. Chem. Soc.* **1982**, *104*, 3269.
(36) Bencini, A.; Gatteschi, D. *J. Am. Chem. Soc.* **1986**, *108*, 5763.
(37) Ross, P. K.; Solomon, E. I. *J. Am. Chem. Soc.* **1991**, *113*, 3246.
(38) Jacobsen, H.; Kraatz, H. B.; Ziegler, T.; Boorman, P. M. *J. Am. Chem. Soc.* **1992**, *114*, 7851.
(39) Mouesca, J.-M.; Chen, J. L.; Noodleman, L.; Bashford, D.; Case, D. A. *J. Am. Chem. Soc.* **1994**, *116*, 11898.
(40) Medley, G. A.; Stranger, R. *Inorg. Chem.* **1994**, *33*, 3976.
(41) Lovell, T.; McGrady, J. E.; Stranger, R.; Macgregor, S. A. *Inorg. Chem.* **1996**, *35*, 3079.
(42) McGrady, J. E.; Stranger, R.; Lovell, T. *J. Phys. Chem. A* **1997**, *101*, 6265.
(43) McGrady, J. E.; Lovell, T.; Stranger, R. *Inorg. Chem.* **1997**, *36*, 3242.
(44) McGrady, J. E.; Stranger, R.; Lovell, T. *Inorg. Chem.* **1998**, *37*, 3802.
(45) (a) Fonseca Guerra, C.; Snijders, J. G.; te Velde, G.; Baerends, E. J. *Theor. Chem. Acc.* **1998**, *99*, 391. (b) *ADF2000.02*; SCM, Theoretical Chemistry, Vrije Universiteit: Amsterdam, The Netherlands, http://www.scm.com.
(46) Vosko, S. H.; Wilk, L.; Nusair, M. *Can. J. Phys.* **1980**, *58*, 1200.
(47) Becke, A. D. *J. Chem. Phys.* **1986**, *84*, 4524.
(48) Perdew, J. P. *Phys. Rev. B* **1986**, *33*, 8822.
(49) Versluis, L.; Ziegler, T. *J. Chem. Phys.* **1988**, *88*, 322.

symmetry group (in the case of di-μ-oxo- and di-μ-hydroxo-bridged diiron(III) substituted γ-silicotungstates) or the D_{2h} symmetry group (in the case of di-μ-oxo- and di-μ-hydroxo-bridged diiron(III) model complexes). A double-ζ Slater type orbital (STO) basis set was employed to describe the valence electrons of Si, O, and H. For W ($n = 6$), double-ζ Slater functions were used for the $(n - 1)$spd and ns shells, whereas the np shell was described by a single orbital. For Fe ($n = 4$), the same quality basis set was employed for the $(n - 1)$sp and $n$sp shells, whereas a triple-ζ function was used to describe the 3d electrons. To obtain the energies and sets of MOs, single-point calculations were performed at the optimized geometries for both spin states using a triple-ζ plus polarization STO basis set for the valence shells of the main group elements (Si, O, and H) and double-ζ Slater functions for the $(n - 1)$sp shells, triple-ζ functions for the $(n - 1)$d and ns shells, and a single STO for the np shell of the transition metals (W and Fe). To generate a BS state, an asymmetry in the initial spin density was introduced for iron atoms bearing the main contributions of spin density in the HS state. By removal of all symmetry elements connecting the two iron centers, the full symmetry (C_{2v} in the case of di-μ-oxo- and di-μ-hydroxo-bridged diiron(III) substituted γ-silicotungstates or D_{2h} in the case of di-μ-oxo- and di-μ-hydroxo-bridged diiron(III) model complexes) was lowered to C_s and C_{2v}, respectively. The shapes of the BS magnetic orbitals were analyzed to identify the superexchange pathways. We think that the use of the HS state optimized geometry in calculations of the BS state properties is a reasonable approximation for the studied systems, as we assume (and it has been previously reported[50] for the diruthenium complex $Ru_2(\mu\text{-}Cl)_2Cl_2(C_5Me_5)_2$) that such systems undergo minor structural changes when a change of spin state occurs.

III. Results and Discussion

(a) Calculation of the Model Dimers. Let us begin with the simple case of di-μ-oxo- and di-μ-hydroxo-bridged diiron(III) complexes with eight water molecules completing the octahedral coordination spheres of the two metal centers (Figure 2). The local (atomic) coordinate frames used herein to describe the atomic and molecular orbitals are chosen so that the z axis at each atom is perpendicular to the plane defined by the $Fe_2(\mu\text{-}O(H))_2$ core and the direction of the y axis is collinear with the Fe−Fe vector.

Geometry Optimization. The main optimized structural parameters for **III** and **IV**, in the HS state, are summarized in Table 1. In both complexes, the two iron atoms have a distorted octahedral coordination environment. The bond lengths increase with decreasing strength of the ligand field and are equal to 1.92 Å for Fe−μ-O (in **III**) and 2.04 Å for Fe−μ-OH (in **IV**), and the average bond lengths between the iron atom and the terminal oxygen atom in its axial and equatorial positions reach 2.12 Å in **IV** and even 2.19 Å in **III**. Due to the trans influence of the oxo or hydroxo ligands, the Fe−O_{eq} bonds are slightly longer than their Fe−O_{ax} analogues. To reduce the repulsion between the two lone pairs on the bridging oxygens, the core in **III** adopts almost square geometry with a Fe−Fe separation of 2.77 Å and Fe−μ-O−Fe bond angles of 92.3°. In **IV**, as a result of the withdrawal of the electron density from the μ-oxygen atoms caused by protonation, the core is expanded along the Fe−Fe axis and constitutes a rhomb with the Fe−Fe distance of 3.29 Å and Fe−μ-O−Fe bond angles of 107.7°. These results quantitatively represent all structural features observed in the complexes synthesized as examples of the di-μ-oxo-bridged diiron(III) core and its protonated analogues.[16,17] Nevertheless, to verify the HS state geometry approximation being used herein, we also carried out geometry optimizations for the BS states of these two complexes. It turned out that the optimization procedure converges to very close geometries, confirming our belief that a reorientation of spins on the metal centers (i.e., a changing of spin state) is accompanied by very minor structural changes.

Table 1. Optimized Structural Parameters for Oxo- and Hydroxo-Bridged Dimers **III** and **IV** (Bond Lengths in Å, Bond Angles in deg)

parameter	dimer **III**	dimer **IV**
Fe−Fe	2.77	3.29
Fe−μO(H)	1.92	2.04
Fe−O_{ax}	2.12	2.08
Fe−O_{eq}	2.25	2.16
μO−Fe−μO	87.7	72.3
Fe−μO−Fe	92.3	107.7
O_{ax}−Fe−Fe	106.8	101.9
O_{ax}−Fe−μO	102.0	99.6
O_{eq}−Fe−μO	80.7	91.7
O_{eq}−Fe−O_{eq}	111.0	104.3

The HS State Electronic Structure. In the oxo-bridged complex, 10 magnetic (unpaired) electrons occupy high-lying α-MOs composed of the symmetrized 3d iron orbitals with or without antibonding participation of the symmetrized 2p μ-oxygen orbitals. Because of the interaction with the MOs corresponding to the terminal (water) oxygen lone pairs and Fe−OH_2 bonds, the weight of symmetrized iron orbitals in the composition of magnetic MOs drops. In the hydroxo-bridged complex, where the electron density on the μ-oxygen atoms and, consequently, the antibonding contributions from the symmetrized 2p μ-oxygen orbitals to the magnetic MOs are reduced upon protonation, the interaction with the symmetrized 2p water−oxygen orbitals appears to be more pronounced. Such a mixing makes the identification and analysis of the magnetic orbitals rather difficult. In contrast, the β-analogues of the magnetic α-MOs can be easily identified. In both complexes, they are represented by the first 10 unoccupied MOs mainly localized on the iron centers. The energies and compositions of these metal-rich MOs for oxo- and hydroxo-bridged complexes **III** and **IV** are summarized in Table 2. The orbitals are shown in Figure 3. The S and A labels are used to indicate symmetric and antisymmetric combinations of the 3d iron orbitals, respectively.

Since the symmetric combinations of both the $3d_{x^2-y^2}$ and $3d_{z^2}$ iron orbitals transform as a_{1g} and their antisymmetric combinations as b_{2u}, the a_{1g}-MO (or the b_{2u}-MO) corresponding to the iron orbitals of one type contains a small admixture

(50) McGrady, J. E. *Angew. Chem., Int. Ed.* **2000**, *39*, 3077.

Table 2. Energies and Compositions (in %) of the HS State β-Orbitals for Oxo- and Hydroxo-Bridged Dimers **III** and **IV** (Labels S and A Mean Symmetric and Antisymmetric Combinations of Iron Orbitals, Respectively)

A. Dimer **III**

level	combination	ϵ (eV)	O_{eq}	O_{ax}	Fe	μ-O
$3a_{1u}$	$(xz)_A$	−11.260	3		96 (xz)	
$6b_{3g}$	$(yz)_A$	−10.811		4	95 (yz)	
$11a_{1g}$	$(x^2-y^2)_S$	−10.725			85 ($\sim x^2-y^2$)	10 (p_x)
$10b_{2u}$	$(x^2-y^2)_A$	−10.647		2	95 ($\sim x^2-y^2$)	
$4b_{2g}$	$(xz)_S$	−10.167			62 (xz)	37 (p_z)
$7b_{1u}$	$(yz)_S$	−10.153		2	65 (yz)	30 (p_z)
$12a_{1g}$	$(z^2)_S$	−10.023		7	77 ($\sim z^2$)	9 (p_x)
$11b_{2u}$	$(z^2)_A$	−9.622		5	76 ($\sim z^2$)	14 (p_y)
$7b_{1g}$	$(xy)_A$	−9.288	4		63 (xy)	23 (p_y)
$8b_{3u}$	$(xy)_S$	−8.834	2		65 (xy)	32 (p_x)

B. Dimer **IV**

level	combination	ϵ (eV)	O_{eq}	O_{ax}	Fe	μ-O
$3a_{1u}$	$(xz)_A$	−20.750	10		89 (xz)	
$10b_{2u}$	$(x^2-y^2)_A$	−20.723		2	96 (x^2-y^2)	
$11a_{1g}$	$(x^2-y^2)_S$	−20.623		2	91 (x^2-y^2)	1 (p_x)
$6b_{3g}$	$(yz)_A$	−20.429		15	83 (yz)	
$4b_{2g}$	$(xz)_S$	−20.314	5		75 (xz)	20 (p_z)
$7b_{1u}$	$(yz)_S$	−19.990	1	7	74 (yz)	17 (p_z)
$8b_{3u}$	$(xy)_S$	−19.752	6		84 (xy)	7 (p_x, s)
$12a_{1g}$	$(z^2)_S$	−19.429	3	11	80 (z^2)	<1 (p_x)
$11b_{2u}$	$(z^2)_A$	−19.212	1	11	77 (z^2)	6 (p_y)
$7b_{1g}$	$(xy)_A$	−18.954	7		67 (xy)	23 (p_y)

from the iron orbitals of the other type. However, this mixing is negligible in the case of the hydroxo-bridged complex.

In Table 3, the energetic differences, $\Delta_i = \epsilon_{Si} - \epsilon_{Ai}$, between the MOs corresponding to the symmetric (S) and antisymmetric (A) combinations of the $3d_i$ iron orbitals are presented. It should be stressed that these MOs originate from the half-occupied 3d iron orbitals. It was shown by Hoffmann et al.[51] that the antiferromagnetic part of the magnetic interactions in weakly coupled dimetallic complexes can be analyzed in terms of the S−A pairs of such MOs, and the squares of the splittings in energy, Δ_i^2, are proportional to the contributions from the corresponding pairs of MOs to the antiferromagnetic component of the exchange coupling constant, J. Thus, the magnitude of the $\epsilon_{Si} - \epsilon_{Ai}$ splittings can serve as a measure of the effectiveness of the superexchange pathways contributing to the molecular antiferromagnetism. By applying Hoffmann's Δ-model, one can gain some first insights into the nature of the antiferromagnetic interactions of a given system. This model was successfully employed in the studies of exchange coupling in simple dimetallic complexes.[20,21,23] Let us analyze the Δ_i values for diiron(III) complexes **III** and **IV** in this context. It is easily seen that, in the oxo-bridged dimer, the presence of the lone pairs on the bridging oxygen atoms generates two efficient superexchange pathways formed by the $3d_{xz}$ and $3d_{yz}$ iron orbitals. The interaction of the $3d_{xz}$ iron orbitals via the $2p_z$ μ-oxygen orbitals is clearly dominant. According to the Δ_i values, the superexchange interactions of the $3d_{xy}$ and $3d_{z^2}$ iron orbitals also give small contributions to the molecular antiferromagnetism. In the hydroxo-bridged dimer, due to the formation of the μ-O−H bonds, the bonding interactions within the core become weaker which gives rise to an expanded rhombic core structure. The symmetrized 2p μ-oxygen orbitals contribute to the set of MOs of interest to a lesser extent, and the antibonding character of these MOs decreases. Thus, the energetic splittings, Δ_i, are smaller (except for $\Delta_{x^2-y^2}$) than those for the oxo-bridged dimer. The largest contribution to the antiferromagnetic interactions comes from the $3d_{xy}$ iron orbitals because of the strong stabilization of the $8b_{3u}$ orbital, where the antibonding contribution from the $2p_x$ μ-oxygen orbitals is reduced by 25%.

In accordance with the previous discussion, the spin density of the oxo-bridged system (**III**) is mainly concentrated within the $Fe_2(\mu\text{-}O)_2$ unit (Table 4); the water−oxygen atoms bear only its minor contributions. In the hydroxo-bridged system (**IV**), the spin density is more delocalized and has increased contributions on the water−oxygen atoms and decreased contributions on the μ-oxygen atoms. The latter result can also be easily predicted from the previous MO analysis.

The BS State Electronic Structure. The BS state atomic spin densities for oxo- and hydroxo-bridged systems **III** and **IV** are given in the Supporting Information. In both dimers, magnetic α- and β-electrons are mainly localized on opposite metal centers; the atomic spin densities on the left and right iron atoms are equal to 4.00 and −4.00 in **III** and 4.19 and −4.19 in **IV**.

In the oxo-bridged complex, five magnetic α-electrons occupy the five highest occupied α-MOs which have main contributions from the first iron atom and μ-oxygen atoms and some small contributions from the second iron atom (Figure 4). Five magnetic β-electrons occupy the five highest occupied β-MOs which are related to their α-counterparts by reflection in the xz plane containing the two bridging oxo ligands, and we do not consider them. The shapes of the magnetic orbitals in Figure 4 indicate that the direct overlap of 3d iron orbitals is negligible in each case; the magnetic properties are dominated by the superexchange interactions between the metal centers. The composition and magnitude of the delocalization tails on the second iron atom reflect the effectiveness of the same-symmetry (d_i−d_i) and mixed-symmetry (d_i−d_j) superexchange pathways. We would like to note that the information regarding the interactions between different types of iron orbitals is not available from the HS calculations, where the full delocalization of magnetic electrons is imposed by the symmetry. In other words, the crossed superexchange pathways cannot be described within the Δ-model. It should be stressed that we deal with the d^5 dimers, and thus, all their superexchange pathways correspond to the interactions of the half-occupied 3d iron orbitals and should give antiferromagnetic contributions to the magnetic coupling.

To identify the superexchange pathways and to assess their relative importance, let us consider in more detail the compositions of the magnetic orbitals of the studied system. In Table 5, we collect the results concerning its magnetic α-MOs and, in addition, the first five unoccupied α-MOs which are mainly centered on the second iron atom. Within

(51) Hay, P. J.; Thibeault, J. C.; Hoffmann, R. *J. Am. Chem. Soc*. **1975**, *97*, 4884.

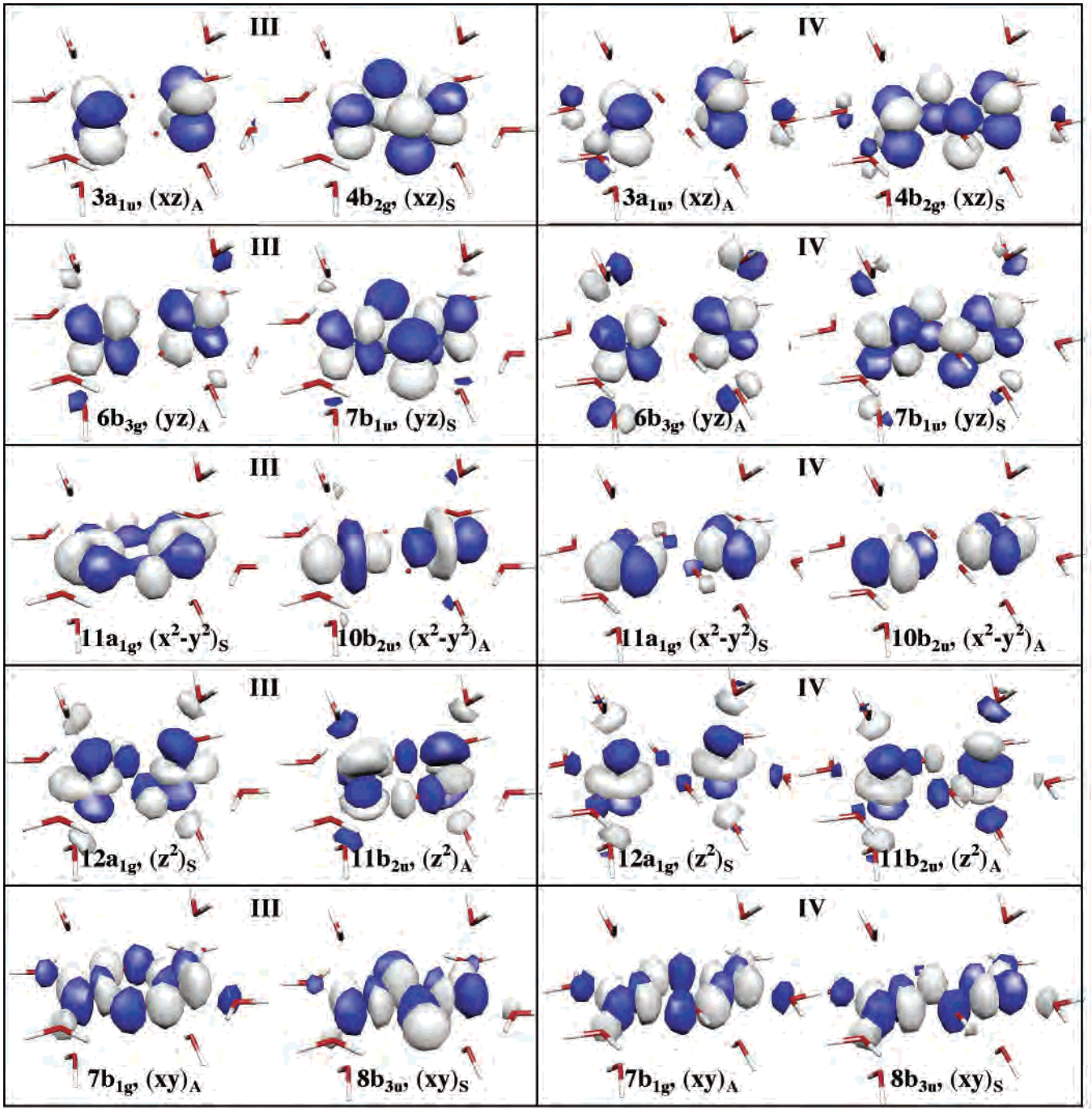

Figure 3. HS state β-orbitals for oxo- and hydroxo-bridged dimers **III** and **I**.

Table 3. HS State Energetic Differences, Δ_i, for Oxo- and Hydroxo-Bridged Dimers **III** and **IV** and Polyanions **I** and **II**

Δ_i (eV)	dimer **III**	dimer **IV**	polyanion **I**	polyanion **II**
Δ_{xy}	0.454	0.798	1.074	0.160
Δ_{z^2}	0.401	0.217	0.377	0.043
$\Delta_{x^2-y^2}$	0.078	0.100	0.658	0.079
Δ_{yz}	0.658	0.439	0.942	0.091
Δ_{xz}	1.093	0.436	0.942	0.279

Table 4. HS State Atomic Spin Densities for Oxo- and Hydroxo-Bridged Dimers **III** and **IV** and Polyanions **I** and **II**

atom	dimer **III**	dimer **IV**	atom	polyanion **I**	polyanion **II**
Fe	4.06	4.23	Fe	3.98	4.10
μ-O	0.79	0.36	μ-O	0.68	0.24
O_{eq}	0.02	0.08	O_{eq}	0.05	0.19
O_{ax}	0.04	0.11	O_{Si}	0.08	0.12
			OH_2	0.01	0.02

the a_2 and b_2 irreducible representations, the occupied and unoccupied MOs ($6a_2$ and $7a_2$ and $12b_2$ and $13b_2$) represent the last two out of three MOs resulting from the interaction of the $3d_{xz,yz}(Fe_1)$, $3d_{xz,yz}(Fe_2)$, and symmetrized $2p_z(\mu\text{-O})$ orbitals. The occupied MOs have antibonding interactions between the $3d_i(Fe_1)$ and $2p_z(\mu\text{-O})$ orbitals and bonding interactions between the $2p_z(\mu\text{-O})$ and $3d_i(Fe_2)$ orbitals. In the unoccupied MOs, both interactions are antibonding. As it follows from Table 5 and Figure 4, namely, the $3d_{xz}$ and $3d_{yz}$ iron orbitals form the most efficient superexchange pathways, and the $xz-xz$ mechanism is clearly dominant, being in agreement with the predictions of the Δ-model.

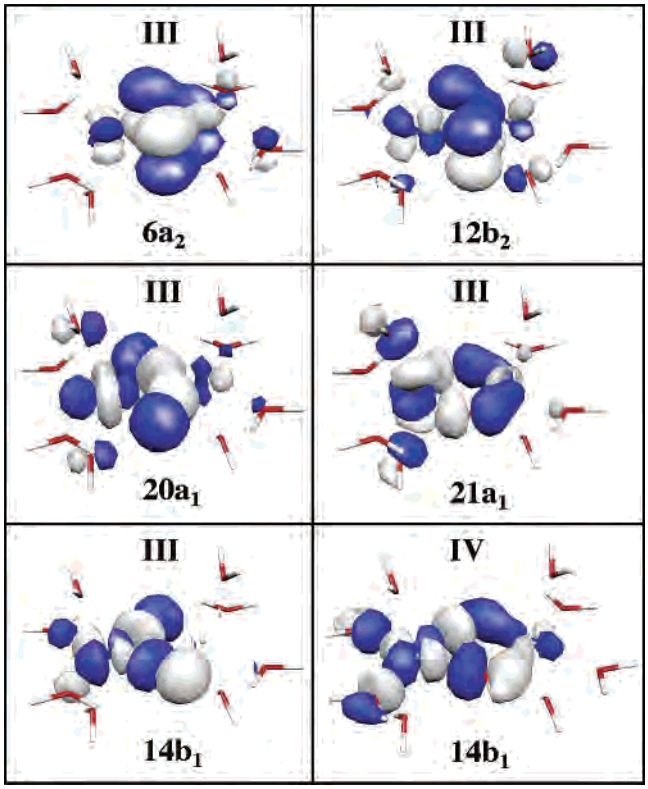

Figure 4. BS state magnetic α-orbitals for oxo- and hydroxo-bridged dimers **III** and **IV**.

Within the a_1 representation, there are two iron orbitals ($d_{x^2-y^2}$ and d_{z^2}) on each metal site and two symmetrized 2p μ-oxygen orbitals, resulting in six MOs. As we can see from Table 5 and Figure 4, the MOs corresponding to the $3d_{x^2-y^2}$ iron orbitals have a small admixture from the $3d_{z^2}$ orbitals and vice versa. Interestingly, the delocalization tail on the second iron atom in the $20a_1$ magnetic orbital corresponding to the $3d_{x^2-y^2}$ iron orbitals has in fact d_{z^2} character, and the delocalization tail in the $21a_1$ magnetic orbital corresponding to the $3d_{z^2}$ iron orbitals mainly consists of the $3d_{x^2-y^2}$ orbital. This means that the crossed pathways $(x^2 - y^2)-z^2$ and $z^2-(x^2 - y^2)$ have a greater significance compared to their symmetric counterparts $(x^2 - y^2)-(x^2 - y^2)$ and z^2-z^2. Nevertheless, even these crossed pathways are not very efficient. Within the b_1 representation, the occupied and unoccupied MOs ($14b_1$ and $15b_1$) represent the last two out of four MOs resulting from the interaction of the $3d_{xy}(Fe_1)$, $3d_{xy}(Fe_2)$, and two symmetrized 2p(μ-O) orbitals. In the occupied (magnetic) orbital, the in-plane 2p(μ-O) orbitals align for an optimal overlap with the $3d_{xy}$ orbital on the first iron atom; however, the distance between the two metal centers appears to be too short to activate the bonding interaction with the $3d_{xy}$ orbital on the second iron atom. Thus, the $3d_{xy}$ iron orbitals in the oxo-bridged complex give a negligible contribution to the superexchange.

In the hydroxo-bridged complex, due to the weakening of the bonding interactions within the core, the set of magnetic orbitals overlaps with the oxygen-based MOs. The magnetic orbitals contain significant contributions from the symmetrized 2p water−oxygen orbitals, and the weight of the iron orbitals drops. Thus, the identification of the magnetic orbitals becomes complicated. Nevertheless, by analyzing the occupied set of MOs, one can conclude that the withdrawal of the electron density from the bridging oxygen atoms and, as a consequence, the increase of the Fe−Fe distance lower the effectiveness of the *xz*−*xz* and *yz*−*yz* pathways and raise the effectiveness of the *xy*−*xy* pathway. The magnetic orbital corresponding to the latter pathway has quite a significant contribution (7%) from the $3d_{xy}$ orbital on the second iron atom (Figure 4). This result is again in agreement with the predictions of the Δ-model. The same-symmetry and mixed-symmetry superexchange interactions of the $3d_{x^2-y^2}$ and $3d_{z^2}$ iron orbitals are negligibly small. However, it is interesting to note that the same-symmetry pathways appear to be somewhat more efficient, since in each case the main contribution on the first iron atom and a small admixture on the second iron atom have the same d character.

The calculated values of the exchange coupling constant, *J*, for the oxo- and hydroxo-bridged complexes are equal to −41 and −43 cm^{-1}, respectively. Surprisingly, despite the core expansion, the exchange coupling between the two iron atoms in the hydroxo-bridged complex is a little bit stronger than the coupling in the oxo-bridged complex. We would like to stress that the experimental *J* values obtained for the $[Fe_2(\mu\text{-O})_2(6TLA)_2]^{2+}$ (−31 cm^{-1}) and $[Fe_2(\mu\text{-O})(\mu\text{-OH})(6TLA)_2]^{3+}$ (−56 cm^{-1}) dimers[16,17] containing the similar core structures also reveal a surprisingly strong exchange coupling in the protonated system.

(b) Calculation of the Diiron Substituted γ-Silicotungstates. Having examined the features of the electronic structure and the nature of the metal−metal interaction in the model di-μ-oxo- and di-μ-hydroxo-bridged diiron(III) complexes, we now consider what peculiarities in the exchange coupling appear after incorporation of such core structures into the POM framework. In this section, we present the results of calculations on the di-μ-oxo- and di-μ-hydroxo-bridged diiron(III) substituted γ-silicotungstates (Figure 1). The local coordinate frames used herein to describe the atomic and molecular orbitals have the *z* axis at each iron atom directed along the $Fe-OH_2$ bond and the *y* axis bisecting the Fe−μ-O bonds. At all oxygen atoms, the *z* axis is perpendicular to the Fe−Fe and μ-O−μ-O vectors, whereas the direction of the *y* axis is collinear with the Fe−Fe vector.

Geometry Optimization. Full geometry optimizations carried out for anions **I** and **II** result in the formation of structures where the terminal water ligands are not bonded with the iron atoms. The water hydrogens start to interact with the neighboring oxygens, weakening the $Fe-OH_2$ bonds and forcing the water ligands to leave the first coordination sphere of the polyanions. Indeed, this means that such highly charged systems do not exist in the gas phase, and the external field generated by the solvent and the counterions is needed to stabilize them. Thus, to take somehow into account the solvent constraints, we performed partial optimizations, keeping the positions of the water molecules frozen. As the mobility of the water ligands even in the

Table 5. Energies and Compositions (in %) of the BS State α-Orbitals for Oxo-Bridged Dimer **III**

			left				right		
level	occ	ϵ (eV)	O_{eq}	O_{ax}	Fe	μ-O	Fe	O_{ax}	O_{eq}
$20a_1$	1	−13.692		6	34 (x^2-y^2)	46 (p_x, p_y)	6 ($\sim z^2$)		
$21a_1$	1	−13.237		14	42 ($\sim z^2$)	27 (p_y)	7 ($\sim x^2-y^2$)		
$12b_2$	1	−13.108	2	2	17 (yz)	57 (p_z)	12 (yz)	6	
$6a_2$	1	−12.999			9 (xz)	67 (p_z)	19 (xz)		4
$14b_1$	1	−11.579	4		31 (xy)	58 (p_x, p_y)	<1 (xy)		
$7a_2$	0	−10.825			<1 (xz)	22 (p_z)	76 (xz)		1
$22a_1$	0	−10.674			<1 (z^2)	11 (p_x, p_y)	84 ($\sim x^2-y^2$)	1	
$13b_2$	0	−10.607			<1 (yz)	16 (p_z)	80 (yz)	2	
$23a_1$	0	−10.015			<1 (x^2-y^2)	6 (p_y)	80 ($\sim z^2$)	7	
$15b_1$	0	−9.229			<1 (xy)	25 (p_x, p_y)	67 (xy)		3

Table 6. Optimized Structural Parameters for Oxo- and Hydroxo-Bridged Polyanions **I** and **II** with the Fe−Fe−OH_2 Bond Angle Fixed at 95, 105, and 115° (Bond Lengths in Å, Bond and Dihedral Angles in deg)

	polyanion **I**			polyanion **II**		
parameter	95°	105°	115°	95°	105°	115°
Fe−Fe	2.69	2.68	2.68	3.02	3.02	3.03
Fe−μO(H)	1.92	1.92	1.92	2.02	2.01	2.01
Fe−O_{eq}	2.07	2.08	2.11	1.92	1.93	1.94
Fe−O_{Si}	2.16	2.19	2.18	2.15	2.12	2.15
Fe−OH_2	2.35	2.27	2.21	2.23	2.21	2.20
Fe−μO−Fe	88.9	88.4	88.6	96.8	97.2	97.4
μO−Fe−Fe−μO	153.8	152.0	149.7	154.5	150.2	147.5

solvent field can be quite high, we tested three different positions with the bond angle Fe−Fe−OH_2 fixed at 95, 105, and 115°. In each case, the experimental geometry of the nonsubstituted γ-silicotungstate was taken as a starting geometry in the optimization procedure. The results of optimizations for both polyanions are summarized in Table 6.

By comparing the data collected in Tables 1 and 6, one can see that the di-μ-oxo(hydroxo)-bridged diiron(III) core units in **I** and **II** reproduce the structural features of the free model dimers quite well. Again, the core in **I** is compressed along the Fe−Fe axis and has almost the same parameters as in **III**; the core in **II** is expanded along the Fe−Fe axis just as in **IV**. However, due to the perturbations caused by the POM framework, the cores in **I** and **II** acquire a new feature. Namely, the cores are no longer planar, as the μ-oxygen atoms are pushed out of the plane by the repulsion with the POM oxygens. This distortion is manifested in the deviation of the dihedral angle μ-O−Fe−Fe−μ-O from 180°. In both polyanions, the alteration of the water ligand positions does not essentially influence the geometry of the cores. All core parameters appear to be almost invariable. The main changes being noticed are the following. The increase of the bond angle Fe−Fe−OH_2 results in a decrease of the Fe−OH_2 bond length and μ-O−Fe−Fe−μ-O dihedral angle. Thus, when the repulsion between the two water molecules decreases, the cores become still more nonplanar.

As the alteration of the water ligand positions results in minor structural changes, the electronic structures of the studied systems in each spin state appear to be almost identical for all three values of the Fe−Fe−OH_2 bond angle. Thus, in the following discussion of the MO structures, we will use the results obtained at the geometries with the Fe−Fe−OH_2 bond angle equal to 95°.

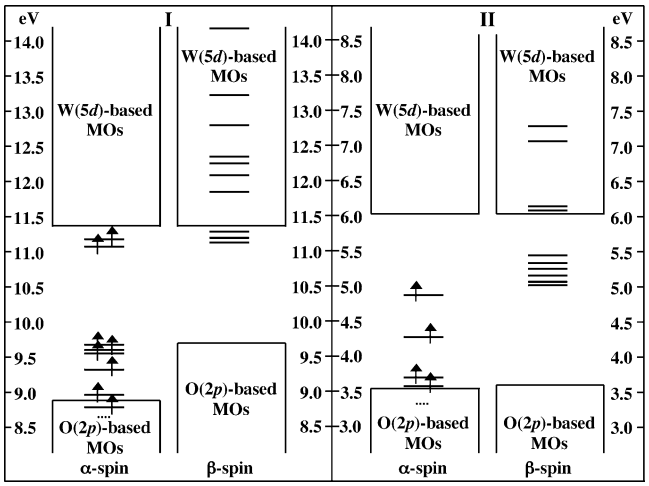

Figure 5. HS state energy diagrams for oxo- and hydroxo-bridged polyanions **I** and **II** (continuous lines represent magnetic α-MOs and their β-counterparts).

The HS State Electronic Structure. The occupied (magnetic) α-MOs and their unoccupied β-counterparts for **I** and **II** mostly resemble those for **III** and **IV**, respectively. In the oxo-bridged anion and to a much greater extent in its protonated analogue, the set of magnetic orbitals overlaps with the oxygen-based MOs, and thus, the magnetic orbitals have additional contributions from the symmetrized 2p POM oxygen orbitals. In both anions, some low-energy magnetic orbitals even dissolve among the oxygen-based MOs and cannot be identified (Figure 5). The β-counterparts of the magnetic orbitals are not perturbed by the interaction with the oxygen-based MOs and are easily identified (Figure 5). These orbitals are shown in the Supporting Information. We present some of them in Figure 6 to demonstrate the main differences between the considered β-MOs in polyanions and simple dimers. The energies and compositions of the β-orbitals for **I** and **II** are summarized in Table 7. As their analogues in **III** and **IV**, these orbitals are composed of the symmetrized 3d iron orbitals and have antibonding contributions from the symmetrized 2p μ-oxygen orbitals which are quite significant in **I** and are much smaller in **II**. The interaction with the symmetrized 2p orbitals of the other oxygens forming the iron coordination spheres is again stronger in the hydroxo-bridged system. It should be stressed, however, that the discussed set of β-MOs in both polyanions (but more strongly in the oxo-bridged system) overlaps with the tungsten-based MOs. As a result, the high-energy orbitals corresponding to the $3d_{xy}$ iron orbitals have contributions

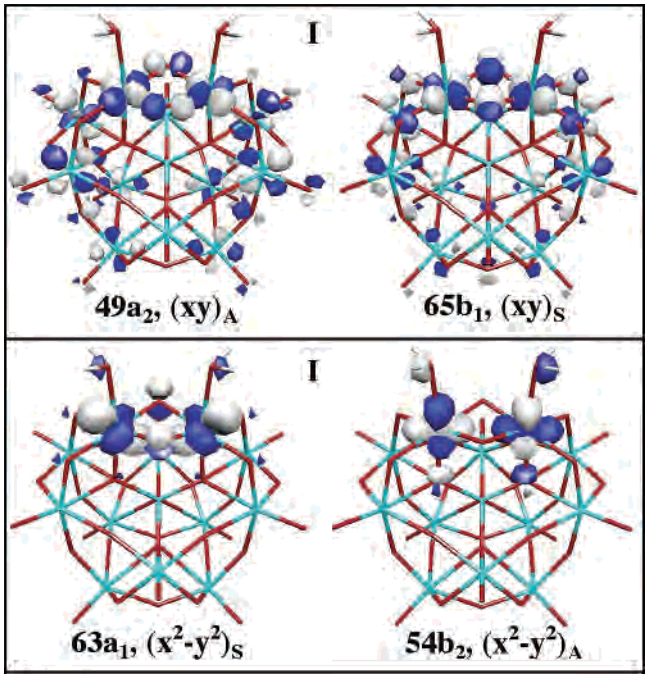

Figure 6. HS state β-orbitals for oxo-bridged polyanion **I**.

Table 7. Energies and Compositions (in %) of the HS State β-Orbitals for Oxo- and Hydroxo-Bridged Polyanions **I** and **II** (Labels S and A Mean Symmetric and Antisymmetric Combinations of Iron Orbitals, Respectively)

A. Polyanion **I**

level	combination	ϵ (eV)	O_{eq}	O_{Si}	OH_2	Fe	μ-O
$43a_2$	$(xz)_A$	11.214	1	2		94 (xz)	
$63a_1$	$(x^2-y^2)_S$	11.225	2			65 ($\sim x^2-y^2$)	7 (p_z, p_x)
$53b_2$	$(yz)_A$	11.392	1			95 (yz)	
$54b_2$	$(x^2-y^2)_A$	11.883	1	4	1	63 ($\sim x^2-y^2$)	
$55b_1$	$(xz)_S$	12.156				49 (xz)	25 (p_z)
$66a_1$	$(yz)_S$	12.334		2		48 ($\sim yz$)	23 (p_z, p_x)
$67a_1$	$(z^2)_S$	12.436		4	2	50 ($\sim z^2$)	4 (p_x)
$58b_2$	$(z^2)_A$	12.813		2	6	42 ($\sim z^2$)	9 (p_y)
$49a_2$	$(xy)_A$	13.255	2			27 (xy)	9 (p_y)
$65b_1$	$(xy)_S$	14.329	8			28 (xy)	10 (p_x)

B. Polyanion **II**

level	combination	ϵ (eV)	O_{eq}	O_{Si}	OH_2	Fe	μ-O
$43a_2$	$(xz)_A$	5.054	4	2		88 (xz)	
$53b_2$	$(yz)_A$	5.062	3			91 (yz)	
$63a_1$	$(yz)_S$	5.153	5			82 (yz)	6 (p_z)
$53b_1$	$(xz)_S$	5.333	4			83 (xz)	7 (p_z)
$64a_1$	$(x^2-y^2)_S$	5.410	11			72 (x^2-y^2)	3 (p_x, p_z)
$54b_2$	$(x^2-y^2)_A$	5.489	9			80 (x^2-y^2)	
$65a_1$	$(z^2)_S$	6.049	3	9	2	69 (z^2)	4 (p_z, p_x)
$55b_2$	$(z^2)_A$	6.092	3	8	2	70 (z^2)	3 (p_y)
$56b_1$	$(xy)_S$	7.107	10			47 (xy)	7 (p_x, p_z, s)
$47a_2$	$(xy)_A$	7.267	5			35 (xy)	9 (p_y)

from the symmetrized 5d tungsten orbitals, and the weight of the iron orbitals drops. This effect is more pronounced in the case of **I** (see Figure 6); the corresponding orbitals in **II** are less perturbed by the interaction with the tungsten-based MOs.

In the oxo-bridged anion, the a_1- and b_2-MOs corresponding to the $3d_{x^2-y^2}$, $3d_{yz}$, or $3d_{z^2}$ iron orbitals are not pure and contain admixtures from the other two iron orbitals. It becomes possible due to their transformation properties (a_1 for symmetric and b_2 for antisymmetric combinations). Such a mixing is very extensive in the pair of MOs corresponding to the $3d_{x^2-y^2}$ iron orbitals (see Figure 6) and is much smaller in the $3d_{z^2}$-based MOs. In the pair of $3d_{yz}$-based MOs, the highest orbital ($66a_1$) is strongly contaminated. In the hydroxo-bridged anion, a symmetry-allowed mixing of iron orbitals is negligible.

The energetic differences, Δ_i, for **I** and **II** are presented in Table 3. In the oxo-bridged anion, the Δ_{xy} and $\Delta_{x^2-y^2}$ values appear to be surprisingly high; the Δ_{yz} value also increases. However, these splittings could be interpreted as indicators of the effectiveness of the corresponding superexchange pathways and reflect the influence of the POM framework on the formation of these pathways only if the Δ-model could be applied to such complicated systems. In the hydroxo-bridged anion, where interactions with the tungsten-based MOs and mixing of the 3d iron orbitals within the a_1- and b_2-MO sets are much weaker, the Δ_i values seem to be reasonable. Apparently, all same-symmetry pathways (including $xy-xy$) should not be very efficient. In this section, however, we do not make any conclusions about the strength of antiferromagnetic exchange and the validity of the Δ-model for our systems. We will consider these problems in the next section, where the relative importance of superexchange pathways will be assessed from the BS calculations.

The HS state spin density of polyanions **I** and **II** is mostly localized on the core units; the POM atoms bear its minor contributions. The atomic spin densities on the core atoms and neighboring oxygen atoms in **I** and **II** are collected in Table 4. As one can see, the distributions of the spin density in oxo-bridged systems **I** and **III** and hydroxo-bridged systems **II** and **IV** are identical. The spin density is mainly concentrated within the core in the former pair and is somewhat delocalized over the neighboring oxygen atoms in the latter.

The BS State Electronic Structure. The BS state atomic spin densities for oxo- and hydroxo-bridged anions **I** and **II** are given in the Supporting Information. As it is observed for simple dimers, the left and right iron atoms in polyanions bear the main contributions of the spin density (3.73 and -3.73 in **I** and 4.02 and -4.02 in **II**).

In the oxo-bridged anion, magnetic spin−orbitals are represented by the five highest occupied MOs of the corresponding spin (Figure 7). The magnetic orbitals (α-set) are shown in Figure 8, and their energies and compositions are summarized in Table 8. Within the C_s symmetry, the $3d_{x^2-y^2}$, $3d_{yz}$, and $3d_{z^2}$ iron orbitals transform as a′, whereas the $3d_{xz}$ and $3d_{xy}$ orbitals transform as a″. That is, the number of possible mixed-symmetry pathways increases. However, their effectiveness (as well as the effectiveness of the same-symmetry pathways) is determined by the extent of overlapping between the iron and μ-oxygen orbitals that can be gained on a given core geometry. To identify significant superexchange pathways and to figure out the changes in the strength of antiferromagnetic coupling produced by the POM framework, let us discuss the compositions of the magnetic orbitals of the studied polyanion.

In the 115a′ orbital corresponding to the $3d_{x^2-y^2}$ iron orbitals, the contribution from the second iron atom is very

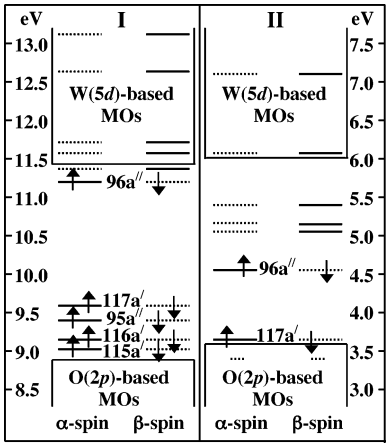

Figure 7. BS state energy diagrams for oxo- and hydroxo-bridged polyanions **I** and **II** (continuous lines represent MOs mainly centered on the first iron atom, and dotted lines represent MOs mainly centered on the second iron atom).

small (only 1%) and in fact contains an admixture from the $3d_{z^2}$ orbital. This means that both the $(x^2 - y^2)-(x^2 - y^2)$ and $(x^2 - y^2)-z^2$ (to say nothing about $(x^2 - y^2)-yz$) pathways are not significant, since in each case efficient orbital overlapping between the μ-oxygen atoms and iron atoms on both sides is not gained. That is, the contributions from these pathways to the metal−metal interaction are even smaller than those in the model dimer **III**. In the 117a′ orbital, the contribution from the second iron atom is mainly d_{yz} in character. Thus, the z^2-yz pathway appears to be more efficient than the z^2-z^2 and $z^2-(x^2 - y^2)$ pathways. As one can see from the shape of this orbital, the $2p_y$ and $2p_z$ μ-oxygen orbitals can align for a quite significant overlap with the iron orbitals on both sides. In other words, the changes in core geometry suppress the $z^2-(x^2 - y^2)$ pathway but activate another one, namely, the z^2-yz pathway. The 116a′ and 95a″ orbitals represent the same-symmetry $yz-yz$ and $xz-xz$ pathways, respectively. The contributions from the second iron atom in these magnetic orbitals are somewhat smaller than those in **III**, as the overlapping between the $3d_{yz}$ or $3d_{xz}$ iron orbitals and $2p_z$ μ-oxygen orbitals on the nonplanar core unit should be less efficient. It follows that the effectiveness of the corresponding pathways in **I** is a little bit smaller. However, the $xz-xz$ mechanism remains more efficient. Finally, the 96a″ magnetic orbital corresponding to the $3d_{xy}$ iron orbitals represents the mixed-symmetry $xy-xz$ pathway which is quite efficient, in contrast to the same-symmetry $xy-xy$ pathway. Thus, the distortions in the core unit do not significantly change the effectiveness of the same-symmetry pathway but allow the formation of a new mixed-symmetry pathway, giving an additional contribution to the superexchange.

In the hydroxo-bridged anion, the sets of magnetic spin−orbitals strongly overlap with the oxygen-based MOs and only two out of five spin−orbitals can be identified within each spin set (Figure 7). These orbitals mostly resemble the corresponding magnetic orbitals in **I** but have much smaller contributions from the μ-oxygen and second iron atoms. Apparently, the magnetic coupling in polyanions **I** and **II** originates from the same superexchange mechanisms, but in **II**, they are less efficient. It should be stressed that on the nonplanar core unit the effectiveness of the $xy-xy$ pathway does not increase upon protonation (see the 96a″ magnetic orbital for **II** in Figure 8). Therefore, the magnetic coupling in **II** should be weaker compared to the case of **I**.

Indeed, the calculated values of the exchange coupling constant, J, for the oxo- and hydroxo-bridged polyanions are equal to -70 and -34 cm^{-1}, respectively. That is, the dependence of the strength of antiferromagnetic exchange on the protonation of the oxo bridges is quite different in simple dimers and polyanions: the exchange coupling increases upon protonation in the former (where the cores are free) and decreases in the latter (where the cores are grafted to the POM matrix). In other words, the distortions in core geometry induced by the POM matrix weaken the exchange interactions in the hydroxo-bridged core unit compared to the oxo-bridged core. It is interesting to note that the same dependence of the strength of magnetic coupling on the protonation of the oxygen-based bridging ligands is observed in the active sites of non-heme iron proteins.[9] This dependence was also evaluated by Noodleman et al.[19] in their density functional study of the cluster models of the $MMOH_{ox}$ and $MMOH_{red}$ active sites. The authors noted that the calculated J values for diiron cores with oxo-, hydroxo-, or aqua-bridging ligands vary inversely in accord with the average Fe−μ-O distance. Thus, both matrixes (inorganic or protein) decrease J upon protonation. However, we would like to stress that such distinct environments should produce quite different distorted core structures. The results of our study clearly demonstrate that the geometry of the whole core unit determines the magnitude of J, and the trends in J values cannot be explained in terms of a single structural parameter.

By comparing the calculated and experimental[4,5] (-5 to -1 cm^{-1}) J values for the diiron(III) substituted γ-silicotungstates, one can conclude that a μ-hydroxo diiron structure is more probable than the di-μ-oxo core unit in the POM system studied by Mizuno et al.[4,5]

It should also be stressed that the Δ-model of Hoffmann et al.[51] cannot describe the exchange coupling in the systems, where a strong symmetry-allowed mixing of metal orbitals takes place and where a dimetallic unit is perturbed by the environment containing the other type of metal atoms. Some limitations of this approach have been mentioned in the literature.[52] Apparently, it can be applied only to simple dimetallic complexes with a symmetry high enough to avoid mixing of metal orbitals.[52]

IV. Conclusions

The antiferromagnetic coupling in diiron cores is sensitive to the distortions in core geometry. Variations in the core structure induced by the environment (such as, for example, POM- or protein matrix) change the significance of superexchange pathways and give rise to new superexchange

(52) Hotzelmann, R.; Wieghardt, K.; Flörke, U.; Haupt, H.-J.; Weatherburn, D. C.; Bonvoisin, J.; Blondin, G.; Girerd, J.-J. *J. Am. Chem. Soc.* **1992**, *114*, 1681.

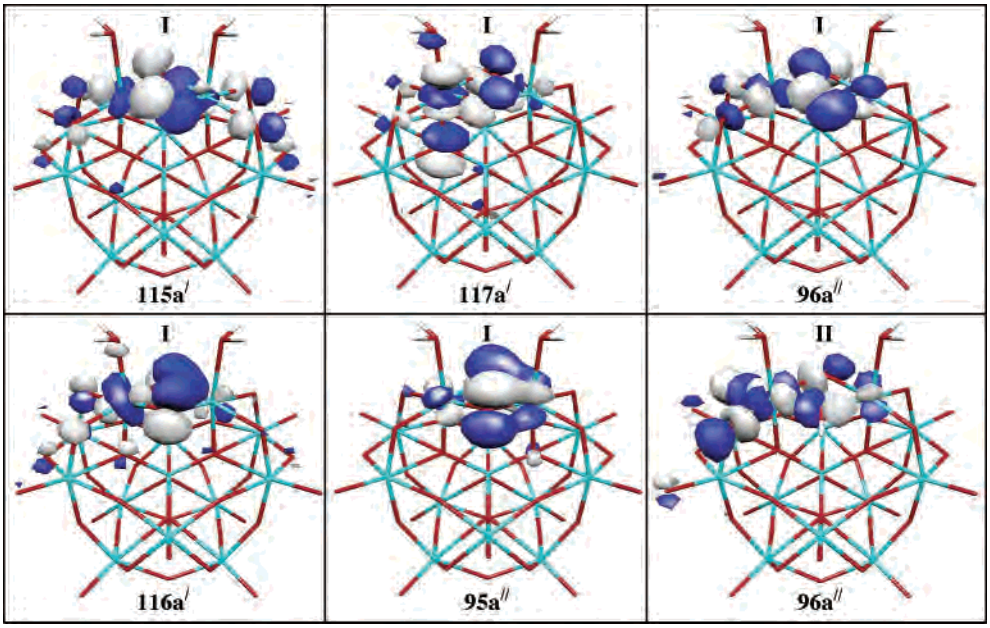

Figure 8. BS state magnetic α-orbitals for oxo- and hydroxo-bridged polyanions **I** and **II**.

Table 8. Energies and Compositions (in %) of the BS State Magnetic α-Orbitals for Oxo-Bridged Polyanion I

		left					right			
level	ϵ (eV)	O_{eq}	O_{Si}	OH_2	Fe	μ-O	Fe	OH_2	O_{Si}	O_{eq}
115a′	9.026	6			21 ($\sim x^2 - y^2$)	40	1			12
116a′	9.170	9	2		26 ($\sim yz$)	37	7 (yz)			1
95a″	9.470				12 (xz)	62	15 (xz)		1	
117a′	9.602	4	22	1	35 (z^2)	18	5 ($\sim yz$)			1
96a″	11.212	6			27 (xy)	37	14 (xz)			

mechanisms. Thus, the strength of antiferromagnetic exchange in dimetallic cores and its dependence on the protonation of the oxo bridges can be quite different in free and grafted core units. Furthermore, the exchange coupling between the magnetic centers in the diiron(III) substituted γ-silicotungstates and the active site of $MMOH_{ox}$ can originate from different superexchange pathways, and therefore, the nature of the antiferromagnetic interactions in these species can be quite distinct. It follows that the conclusions about the structure of the core bridges (oxo, hydroxo, or aqua) in transition metal substituted POM systems, non-heme metalloenzymes, and simple model dimers on the basis of comparison of their J values should be done with care.

Acknowledgment. This work was supported by the CNRS research grant for E.M.Z. The authors thank J. E. McGrady for useful discussion.

Supporting Information Available: Four tables containing the optimized Cartesian coordinates of systems **I**−**IV**, one table showing the BS state atomic spin densities for **I**−**IV**, and one figure showing the HS state β-orbitals for **I** and **II**. This material is available free of charge via the Internet at http://pubs.acs.org.

IC035161T